Riparian vegetation distribution induced by river flow variability: A stochastic approach

Riparian vegetation distribution induced by river flow variability: A stochastic approach

C. Camporeale[1] and L. Ridolfi[1]

Received 30 January 2006; revised 3 May 2006; accepted 6 June 2006; published 12 October 2006.

[1] Riparian vegetation is part of one of the most diverse and fragile ecotones. The key role played by river discharge on the dynamics of riparian vegetation has been widely studied and documented. However, although randomness is a fundamental characteristic of river hydrology, very few quantitative vegetation studies take into account the random nature of river discharge. Here we propose a stochastic model of riparian vegetation ecosystem dynamics forced by random variations in river discharge. The model is solved, and the analytical expressions of the probability density function of the overall vegetation biomass and its first moments are obtained. These theoretical results are used to investigate the effect of river hydrology on the distribution of vegetation along the riparian transect transverse to the river. In particular, the influence of the type of riparian species and the statistical characteristics of discharge time series are discussed and compared with field observations.

Citation: Camporeale, C., and L. Ridolfi (2006), Riparian vegetation distribution induced by river flow variability: A stochastic approach, *Water Resour. Res.*, *42*, W10415, doi:10.1029/2006WR004933.

1. Introduction

[2] Riparian vegetation is a type of plant community growing close to river banks [*Naiman and Decamps*, 1997; *Hughes*, 1997; *Mitsch and Gosselink*, 2000]. It is part of a complex ecotone, called the riparian zone, which is "a transitional semiterrestrial area regularly influenced by fresh water, usually extending from the edges of water bodies to the edges of upland communities" [*Naiman et al.*, 2005, p. 2]. Unlike upland vegetation, riparian vegetation is greatly influenced by the fluvial hydrological regime, through the control exerted by the river on water table depth, flooding, and hyporheic fluxes [*Mitsch and Gosselink*, 2000; *Jones and Mulholland*, 2000]. The spatial patterns of riparian vegetation are an evident indication of this strong influence: sparse vegetation is mainly associated with high river discharge variability, e.g., the vegetation is removed by intense floods or wilt during dry periods [*Nanson et al.*, 2002], while uniform vegetation is instead typical of more regular river flow conditions.

[3] In recent years, several field studies have investigated the sensitivity of the riparian vegetation to river-induced disturbances. For example, *Osterkamp and Hupp* [1984] and *Hupp and Osterkamp* [1985] investigated the relationships between riparian vegetation patterns and fluvial landforms, *Mahoney and Rood* [1998] identified the geomorphological features of locations in which seedlings are most likely to germinate and survive, and *Bendix and Hupp* [2000] observed that the species are sorted along gradients in water table depth and unit stream power. *Johnson* [2000] carried out an extensive demographic analysis of the effects of river discharge on tree recruitment and seedling mortality [see also *Bradley and Smith*, 1986; *Auble et al.*, 1994; *Friedman and Auble*, 1999; *Lite et al.*, 2005].

[4] These field works have clearly shown that flooding and the depth of the water table are the two fundamental mechanisms through which river hydrology controls the riparian vegetation evolution. Flood events cause the so-called inundation of a plot, during which a vegetated site is submerged by the stream. Vegetation may benefit from floods, which supply moisture, seeds and nutrients [*Naiman and Decamps*, 1997], though floods are more often known for their negative impact on vegetation, due to physical damage [*Yanosky*, 1982], uprooting and sediment removal [*Osterkamp and Costa*, 1987], anoxia [*Kozlowski*, 1984; *Stevens and Waring*, 1985; *Naumburg et al.*, 2005], and burial [*Hupp*, 1988; *Friedman and Auble*, 1999]. An exposure period instead occurs when the free surface of the river is lower than a vegetated site. In these conditions, the river affects the growth rate of vegetation by controlling the groundwater flow [*Scott et al.*, 1999]. This aspect is very important in semiarid area, e.g., the southwest of the United States and Mediterranean regions, which support phreatophytes that tap the groundwater. On the other hand, in humid areas the groundwater levels have little bearing on vegetation distribution. In the following, we will focus on the former areas, even though, as shown in section 4.1, humid areas can be considered as a particular case where only the influence of the inundation periods is retained.

[5] Even though random variability is a key characteristic of the river hydrology which plays a crucial role in the evolution of riparian vegetation [*Tockner et al.*, 2000; *Stromberg*, 2001; *Steiger et al.*, 2005], the impact of stochastic hydrologic fluctuations on the dynamics of riparian vegetation ecosystems remains for most part poorly

[1]Dipartimento di Idraulica, Trasporti ed Infrastrutture Civili and Water and Environment Research Center, Politecnico di Torino, Turin, Italy.

0043-1397/06/2006WR004933$09.00

understood [*Scott et al.*, 1999; *Lytle and Merritt*, 2004]. Some conceptual qualitative models [*McKenney et al.*, 1995; *Richter and Richter*, 2000; *Gurnell et al.*, 2001] and regression analyses between vegetation growth and river discharge [*Stromberg and Patten*, 1991], or inundation duration [*Franz and Bazzaz*, 1977; *Auble et al.*, 1994], account for some probabilistic aspects of hydrological variability (e.g., frequency, intensity, or duration of the inundation). However, these studies do not explicitly address riparian vegetation dynamics using an approach that is both process based and probabilistic. Moreover, the lack of analytical models limits the study of riparian vegetation to numerical model simulations [e.g., *Pearlstine et al.*, 1985; *Brookes et al.*, 2000; *Lytle and Merritt*, 2004]. If this allows a detailed description of the processes, it makes very difficult to catch general aspects nevertheless. Here we propose a new approach to study the distribution of phreatophyte riparian vegetation, using a stochastic process to model the random forcing exerted by river flow on the dynamics of the overall biomass of vegetation.

[6] The purposes of the present work are (1) to formulate and solve a process-based stochastic model of riparian vegetation dynamics and (2) to investigate the role of the flow variability on the vegetation distribution along a riparian transect. To these aims, we use a minimalistic approach which accounts for the key hydrologic and ecosystem processes, while keeping the model mathematically tractable. A number of simplifications are adopted in the representation of hydrologic and vegetation dynamics. In particular, we maintain steady river morphology and neglected sediment erosion and deposition. Analytical solutions for the steady state probability density function of the vegetation biomass and its main statistics are obtained. Their dependence on the distance from the river, the transect topography, the statistical properties of the river discharge, and the type of vegetation are then elucidated. These analytical results are used to assess to what extent river hydrology is able to affect the distribution of riparian vegetation and explain observed patterns of vegetation distribution.

2. Stochastic Model

[7] The scope of our study is to describe the key processes of riparian vegetation dynamics focusing on the stochastic influence of the river. In order to obtain a representative but mathematically tractable model, some simplifying hypotheses are introduced. First, we refer to the overall vegetation biomass of phreatophyte riparian species, neglecting interspecific interactions [see also *Lytle and Merritt*, 2004; *Perucca et al.*, 2006]. Second, we consider a steady river morphology and, then, geomorphological processes, such as sedimentation and erosion, are neglected [e.g., *Auble et al.*, 1994]. It follows that the model is not able to describe the feedback mechanisms of the vegetation on the site topography. Finally, we neglect the time delay between the vertical movements of the free surface in the river and the water level in the adjacent unconfined aquifer beneath the riparian vegetation. This assumption is reasonable because the delay is generally shorter than the typical timescale of vegetation-groundwater interactions.

[8] The links between the river and the processes that affect age, species and community structure generally develop at the reach scale, namely between the bar form scale and the corridor scale [*Richards et al.*, 2002]. Thus we assume, as a typical spatial scale of the problem, a transversal width of the riparian zone of the order of the mean half width of the river, $\overline{b^*}$ (the star indicates dimensioned quantities), corresponding to the mean water level in the river (see Figure 1). The results of the model are therefore also valid for a curved reach provided the curvature is much lower than $1/\overline{b^*}$, a condition that is very commonly met in meandering rivers [e.g., *Ikeda and Parker*, 1989; *Camporeale et al.*, 2005]. The temporal scales described in the model range from a day, to account for the effect of flooding, to several years, to allow for vegetation growth. As some simplifications affect the shortest scales, the outcomes of the model are interpreted in the long-term, by investigating the steady state conditions.

[9] Let us consider the generic riparian transect shown in Figure 1 and assume the minimum water level in the river (which can be different from zero) as the vertical datum. The free surface oscillates randomly above this level, according to the hydraulic and hydrologic characteristics of the river. The following dimensionless variables are introduced

$$x = \frac{x^* - \overline{w^*}}{\overline{w^*}}, \quad h = \frac{h^* - \overline{h^*}}{\overline{h^*}}, \quad \zeta = \frac{\zeta^* - \overline{h^*}}{\overline{h^*}}, \quad \eta = \frac{\eta^* - \overline{h^*}}{\overline{h^*}}, \tag{1}$$

where x^* is the transversal coordinate, with origin in the intersection between the minimum water level and the river bed, w^* is the river width referred to the x^* coordinate, while h^*, ζ^*, and η^* are the river water level, the phreatic surface position and the bed topography elevation, respectively, referring to the vertical datum (see Figure 1). The bar in relationships (1) indicates the time averaged values; therefore $\overline{w^*}$ marks the mean transversal position of the bank ($\overline{w^*} \equiv \overline{b^*}$ when the minimum river discharge is zero) and $\overline{h^*}$ is the average water level in the river. The function $\eta = \eta(x)$ gives the transect topography, while function $\zeta = \zeta(x, h)$ describes the spatial shape of the phreatic surface and its dependence on the water level in the river. Both $\eta(x)$ and $\zeta(x, h)$ are input data of the problem. As h is a time random variable, $\zeta(x, h)$ and the local depth of the phreatic surface, $\delta(x, h) = \eta(x) - \zeta(x, h)$, are also random variables.

[10] The randomness of the river water levels is described by the probability distribution function (pdf), $p(h)$, and the autocorrelation function, $\rho_h(s^*) = \overline{h(t^*)h(t^* + s^*)}/\overline{h^2(t^*)}$, where s^* is the time delay. This latter function is a key characteristic of the hydrology of a river [e.g., *Bras*, 1990; *Maidment*, 1993] and it can be summarized by the integral scale τ^*, defined as the area of the autocorrelation function $\rho_h(s^*)$, i.e., $\tau^* = \int_0^\infty \rho_h(s^*)\, ds^*$. This scale can be interpreted as the "memory" of the river discharge time series.

[11] The riparian vegetation dynamics are described according to the following model

$$\frac{dv}{dt^*} = -\alpha_1 v^n, \quad h \geq \eta \tag{2a}$$

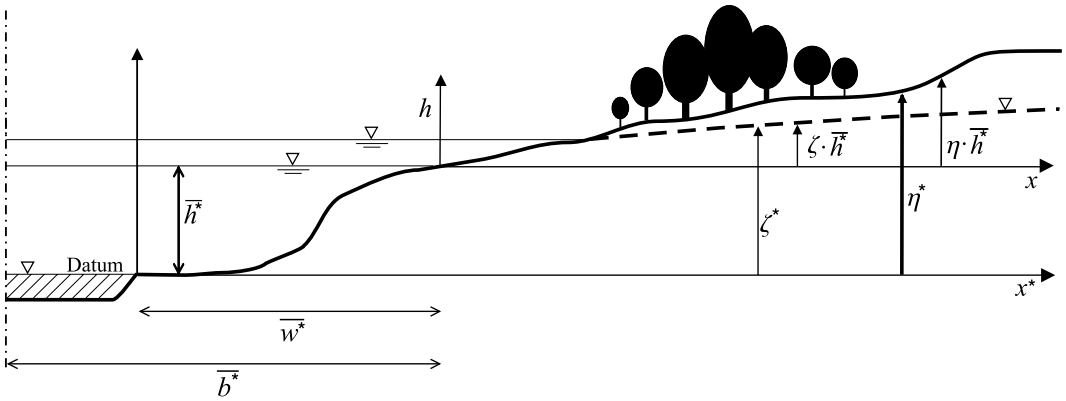

Figure 1. Sketch of the riparian transect and main variables adopted. The dashed line indicates the phreatic surface.

$$\frac{dv}{dt^*} = \alpha_2 v^m (V_c - v)^p, \qquad h < \eta, \tag{2b}$$

where v is the dimensionless vegetation biomass ($v = 1$ in optimum steady conditions), t^* is time, $V_c = V_c(\delta)$ is the dimensionless carrying capacity, i.e., the maximum sustainable biomass, which depends on the depth of the aquifer water table, δ, and α_1 is a coefficient that describes the magnitude of the damage to the vegetation by the flood. Finally, the exponents (n, m, p) and the intrinsic rate of growth, α_2 [*Kot*, 2001], are numerical constants that depend on the characteristics of the vegetation.

[12] Equation (2a) models the decay of the vegetation biomass caused by flooding and assumes that the eventual beneficial influences are overcome by the detrimental processes (i.e., anoxia, burial, uprooting, etc.), as is usual in riparian environments with constant channel morphology [*Auble et al.*, 1994]. Accordingly, a decay timescale, T_d^*, can be defined as the time necessary for the vegetation to decline by 90% (i.e., from $v = 0.95$ to $v = 0.05$). The exponent, n, modulates vegetation response to stream-induced disturbances. For example, $n = 1$ implies an exponential decrease, and when $n < 1$ the models allows the resistance of vegetation to disturbance to increase with the age of vegetation [*Friedman and Auble*, 1999; *Lytle and Merritt*, 2004]. The coefficient α_1 is assumed to be an increasing function of h, with $\alpha_1 = 0$ at $h = \eta$. In fact, higher water levels are associated with stronger vegetation stress, due both to mechanical disturbance and to anoxic conditions. Because the mechanical effect of the stream water on vegetation is proportional to the tangential stress on the bed [*Friedman and Auble*, 1999], while anoxic conditions increase with the water level, both mechanisms are modeled linearly dependent on the submerged depth $h - \eta$,

$$\alpha_1 = K \cdot (h - \eta) \tag{3}$$

where K is a positive empirical coefficient that depends on the vegetation type.

[13] Equation (2b) is a generalization of the commonly used Verhulst-logistic function [*Hunt*, 1982] and it simulates the growth of a phreatophyte species tapping the groundwater [*Botkin et al.*, 1972; *Liu and Ashton*, 1995]. Suitable choices of the exponents m and p and the growth rate α_2 allow equation (2b) to fit a wide variety of mathematical formulations proposed to describe the vegetation growth. An example is the JABOWA forest growth equation derived from *Botkin et al.* [1972; see also *Shugart and West*, 1977; *Pearlstine et al.*, 1985]. These authors modeled vegetation growth under optimum conditions (i.e., $V_c = const = 1$), as

$$\frac{d\vartheta}{dt^*} = \frac{G(\vartheta D_m^*)^{q-1}\left[(\vartheta^3 - 2\vartheta^2 + 1)H_m^* - (\vartheta - 1)^2 \vartheta H_0^*\right]}{2\left[H_0^* + \vartheta(2\vartheta - 3)(H_0^* - H_m^*)\right]H_m^*}, \tag{4}$$

where $\vartheta = D^*/D_m^*$ is the dimensionless diameter, with D^* being the vegetation diameter at breast height H_0^* (conventionally set to 137 cm) and D_m^* its maximum value. H_m^* is the maximum vegetation height, and G and q are two parameters. Generally, G is taken in a way that the vegetation grows to $2H_m^*/3$ at one-half of its maximum age, T_m^*, while q is an allometric exponent that depends on the species and site conditions and varies between 1.5 and 3 [*Baskerville*, 1965; *Perry et al.*, 1969; *Young et al.*, 1980]. Values of H_m^*, D_m^*, and T_m^* are listed in Table 1 for some typical riparian species.

[14] The generalized logistic equation (2b) fits very well the temporal behavior described by the differential equation (4). For example, Figure 2 shows a comparison between four different Botkin growth curves and the corresponding curves fitted to equation (2b). The values of α_2 obtained through curve fitting (fitting errors <10%) are reported in Table 1 for a number of riparian species in the case $q = 2.5$ and $m = p = 1$. Because of the versatility of equation (2b), other laws of vegetation growth can also be fitted by (2b) [e.g., *Liu and Ashton*, 1995].

[15] The carrying capacity, V_c, depends on the depth of water table: phreatophyte species generally have a maximum growth (i.e., $V_c = 1$) when the water table is equal to an optimum depth, δ_{opt}^*, while the water uptake capacity is significantly reduced for groundwater levels that are either too low or too high (e.g., for Salix Alba $\delta_{opt}^* = 0.5$ m, see section 4.2). In fact, because deeper groundwater is out of reach of tap roots, xylem cavitation and stomal closure occur [*Naumburg et al.*, 2005]. On the other hand, shallow water tables are associated with water logging conditions and reduced respiration and gas exchange in the root zone [*Kozlowski*, 1984; *Ridolfi et al.*, 2006]. It follows that there

Table 1. Ecological Parameters for Different Bottomland Hardwood Species[a]

Species Name	Common Name	D_m^*, m	H_m^*, m	T_m^*, years	δ_{opt}^*, m	α_2, $\times 10^5$ d^{-1}
Carya tomentosa	mockernut hickory	1.3	33	300	0.3	6.5
Liriodendron tulipifera	yellow poplar	1.0	15	300	0.6	8.0
Nyssa aquatica	water tupelo	2.5	30	300	0.0	6.5
Populus deltoides	eastern cottonwood	3.5	55	150	1.0	13
Prunus serotina	wild cherry	2.0	40	250	1.1	7.8
Salix nigra	black willow	0.9	12	70	0.5	28

[a]Here $m = p = 1$; $q = 2.5$.

is a range of water table depths, $[\delta_1^*, \delta_2^*]$, that allows vegetation growth, while outside this range, plants are not able to survive. Coherently with this picture, the (dimensionless) carrying capacity reaches its maximum value ($V_c = 1$) at the optimum depth, δ_{opt}^*, and is zero outside the previously mentioned interval. We have modeled this behavior with a parabolic function [see also *Phipps*, 1979; *Pearlstine et al.*, 1985], which in the present dimensionless framework, reads as

$$V_c = V_c(\delta) = \begin{cases} 1 - a(\delta - \delta_{opt})^2 & \delta_1 \le \delta \le \delta_2 \\ 0 & \delta < \delta_1 \quad \text{or} \quad \delta > \delta_2, \end{cases} \tag{5}$$

with $\delta_{opt} = \delta_{opt}^*/\overline{h^*}$ and $a = a^* * \overline{h^*}^2$, where a^* is a constant that we take equal to 0.055 [e.g., *Phipps*, 1979]. Consequently,

$$\delta_{1,2} = \delta_{opt} \mp \sqrt{a}. \tag{6}$$

[16] Through the dependence $V_c = V_c(\delta)$ (i.e., equation (5)), model (2) accounts for the decay of vegetation biomass, due to water stress driven by changes in the phreatic water table, in addition to the decay induced by floods (equation (2a)). Considering the optimum condition, $V_c = 1$, the growth timescale T_g^* is here defined as the time necessary for vegetation to undergo an overall growth, from $v = 0.05$ to $v = 0.95$ [*Perucca et al.*, 2006].

[17] The randomness of the hydrological forcing acts on the vegetation dynamics (equation (2)) in two different ways. First, the sign of $h-\eta$ controls the switching between equations (2a) and (2b), i.e., phases of inundation are alternated with phases of exposure. The statistical characteristics of the switching depend on the probability distribution and autocorrelation function, $p(h)$ and $\rho_h(s^*)$, of h. Second, both quantities α_1 and V_c depend on the random variable h. Thus the model (2)–(5) describes the stochastic evolution of riparian vegetation at any point of a transversal transect for given probabilistic properties of the river flow (i.e., $p(h)$ and $\rho_h(s^*)$), vegetation characteristics (n, m, p, K, α_2, δ_1, and δ_2), section geometry ($\eta(x)$), and geometry of the phreatic surface ($\zeta(x, h)$).

3. Analytical Solution

[18] In order to obtain the analytical expression of the steady state pdf of the vegetation biomass, the functions $\alpha_1 = \alpha_1(h - \eta)$ and $V_c = V_c(\delta)$ are approximated in any plot with their x-dependent probability-averaged values, that is,

$$\langle \alpha_1 \rangle = \frac{1}{P_I} \int_{\eta(x)}^{\infty} \alpha_1 p(h) dh, \tag{7a}$$

$$\langle V_c \rangle = \frac{1}{P_E} \int_{-1}^{\eta(x)} V_c p(h) dh, \tag{7b}$$

where

$$P_I(x) = \int_{\eta(x)}^{\infty} p(h) dh, \tag{8a}$$

$$P_E(x) = \int_{-1}^{\eta(x)} p(h) dh \tag{8b}$$

are the probabilities of inundation and exposure, respectively. Since the pdf of the river levels, $p(h)$, the cross-section geometry of the bank, $\eta(x)$, and the phreatic surface, $\zeta(x, h)$, are the input data of the problem, the quantities $\langle \alpha_1 \rangle$ and $\langle V_c \rangle$ can be evaluated. These depend on (1) the coordinate x along the transect, (2) the probability distribution of water levels, $p(h)$, and (3) the type of vegetation, through the parameters K, δ_{opt} and a. Once $p(h)$ is assigned, the exposure probability, P_E, is univocally linked to x, i.e., P_E can be interpreted as a surrogate variable of the lateral coordinate, x. Finally, P_I is the dimensionless fractional time in which a site at the bottomland is inundated, and is also known as the inundation duration

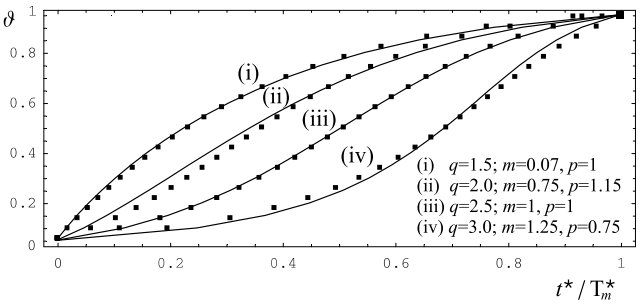

Figure 2. Comparison between different shapes of the JABOWA-forest growth equation (4) and the corresponding curves fitted by model (2b) (dots) in the case of *Salix Nigra*. The fitting parameters are also reported.

or flow duration by field workers [e.g., *Auble et al.*, 1994; *Hupp and Osterkamp*, 1985].

[19] By introducing relationships (7) and (8) into model (2a) and (2b), then dividing by α_2, and scaling the time according to $t = \alpha_2 t^*$ (and then $\tau = \alpha_2 \tau^*$), the following analytically more tractable model is obtained

$$\frac{dv}{dt} = -\alpha v^n, \quad h \geq \eta, \tag{9a}$$

$$\frac{dv}{dt} = v^m(\beta - v)^p, \quad h < \eta, \tag{9b}$$

where

$$\alpha = \frac{\langle \alpha_1 \rangle}{\alpha_2} = \frac{K\langle h - \eta \rangle}{\alpha_2} = k\langle h - \eta \rangle, \qquad \beta = \langle V_c \rangle \tag{10}$$

are two known quantities that depend on position of the site along the transect. At the end of this section, it will be numerically verified how the approximations contained in model (9) do not significatively alter the steady state solution with respect to the original model (2).

[20] Model (9) retains the influence of the random oscillations of the river water level on the vegetation dynamics in the switching between decay phases and growth phases, that alternatively occur in a random (but correlated) way. Therefore, because of the stochastic character of the forcing, the outcome of model (9), herein adopted to describe the riparian vegetation biomass dynamics, is not a deterministic value but a random quantity described by a probability distribution function. The stochastic character of the switching permits model (9) to be expressed by a single stochastic differential equation

$$\frac{dv}{dt} = f(v) + \xi(t)g(v) \tag{11}$$

where $\xi(t)$ is a dichotomic Markov process [*Van Kampen*, 1992] that switches between values Δ_I (inundation) and Δ_E (exposure), and functions $f(v)$ and $g(v)$ are such that equation (11) reduces to equations (9a) and (9b) depending on the value of $\xi(t)$. This yields

$$f(v) = \frac{\Delta_I v^m(\beta - v)^p + \alpha \Delta_E v^n}{\Delta_I - \Delta_E}, \tag{12}$$

$$g(v) = \frac{\alpha v^n + (\beta - v)^p v^m}{\Delta_E - \Delta_I}. \tag{13}$$

[21] Thus we can use the theory of stochastic differential equations driven by multiplicative dichotomic noise [*Kitahara et al.*, 1980; *Van Den Broeck*, 1983] to investigate the dynamics of riparian vegetation. To this aim and without any loss of generality, it can be assumed that the dichotomic noise, $\xi(t)$, has a vanishing average value. Consequently, the average durations of the inundation and exposure periods (T_I and T_E, respectively) satisfy equations [*Van Den Broeck*, 1983]

$$T_E\Delta_E + T_I\Delta_I = 0, \quad \frac{P_{\Delta_I}}{P_{\Delta_E}} = \frac{T_I}{T_E}, \quad \frac{1}{\tau_{DP}} = \frac{1}{T_E} + \frac{1}{T_I}, \tag{14}$$

where $P_{\Delta E}$ and $P_{\Delta I}$ (with $P_{\Delta I} + P_{\Delta E} = 1$) indicate the probability of the dichotomic process of being in state Δ_E or Δ_I, respectively, and τ_{DP} is its integral scale. Without any loss of generality, in the following we set $\Delta_I = 1$.

[22] The dichotomic noise, $\xi(t)$, results to be characterized by only two independent parameters, that we chose to be τ_{DP} and $P_{\Delta I}$. In order for the noise to capture the stochastic structure of the hydrological forcing correctly we assume

$$\tau_{DP} = \tau \qquad P_{\Delta_I} = P_I, \tag{15}$$

namely the memory of the noise is the same as in the river discharge time series and the probability that $\xi(t) = \Delta_I$ (i.e., model (11) coincides with equation (9a)) is equal to the inundation probability (hence $P_{\Delta E} = P_E$).

[23] The solution of the Fokker-Plank equation corresponding to (11) is the pdf of the vegetation density, $\mathcal{P}(v, t)$. Its steady state function (a fundamental property of the Fokker-Plank equation is that all solutions tend to the stationary solution when $t \to \infty$ [*Van Kampen*, 1992, p. 104]) $p(v) = \mathcal{P}(v, t \to \infty)$ can be obtained according to *Kitahara et al.* [1980] and reads

$$p(v) = N\frac{g(v)}{\Phi(v)} \exp\left[-\frac{1}{\tau}\int \frac{f(v')}{\Phi(v')}dv'\right] \tag{16}$$

where N is a normalization constant (i.e., $\int_0^\infty p(v)dv = 1$) and

$$\Phi(v) = [f(v) + \Delta_I g(v)][f(v) + \Delta_E g(v)]. \tag{17}$$

[24] The solution of the integral in equation (16) differs according to the value of the coefficients (n, m, p). In the following, we focus on the case that corresponds to the usual choice $m = n = p = 1$, which refers to the original Verhlust logistic model for growth and the exponential form for decay. Other cases are reported in Appendix A. By substituting equations (12) and (13) in (16) we obtain the steady state pdf of the vegetation biomass

$$p(v) = \frac{N}{\alpha} v^{\frac{\beta(1-\alpha\tau)-(\alpha+\beta)P_I}{\alpha\beta\tau}} (\beta - v)^{\frac{P_I}{\beta\tau}-1}(\alpha + \beta - v), \tag{18}$$

with $v \in [0, \beta]$. It is worth recalling that the pdf of the vegetation biomass depends on the transversal position, x, through the inundation probability, P_I, the coefficient α, and the expected value of the carrying capacity, β. Expression (18) is valid provided

$$P_I < \frac{\beta}{\alpha + \beta}, \tag{19}$$

otherwise N diverges and $p(v)$ tends to $\delta(v)$, where $\delta(\cdot)$ is the Dirac delta function. Since α, β and P_I depend on the

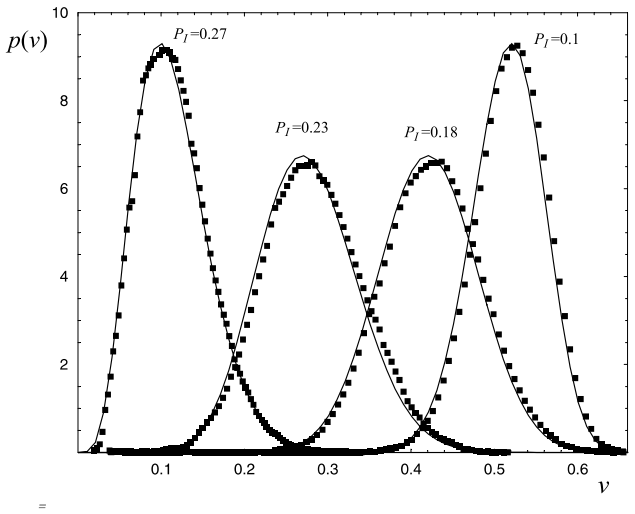

Figure 3. Comparison of analytical expression (18) of the probability distribution, $p(v)$ (solid line), and the pdf obtained from numerical simulations of model 2 (points) for four values of inundation probability, P_I ($\tau = 7.8 \times 10^{-3}$, $C_h = 0.5$, $k = 5$).

bed elevation η through equations (7) and (8a), it results that condition (19) can be used to find the lowest topographic limit of the vegetated zone, and the extension of the riparian zone. It is interesting to observe the such limits do not depend on the correlation time, τ.

[25] Relationship (18) allows one to obtain the analytical expression of its first four moments (i.e., mean, standard deviation, skewness and kurtosis), that are useful to summarize the main statistical characteristics of the stochastic outcome of model (9). For example, again for the case of $m = n = p = 1$ and under condition (19), the expected value is

$$\mu_v = \int_0^\beta v p(v) dv = \frac{\beta \rho_1 (\beta \varepsilon_2 \sigma_1 - \varepsilon_1 \rho_0 \sigma_2)}{(\beta \varepsilon_1 \rho_1 - \rho_0 \rho_2 \sigma_1) \sigma_2}, \qquad (20)$$

where

$$\rho_0 = \alpha + \beta, \quad \rho_1 = \Gamma\left[\frac{1 - P_I}{\alpha\tau}\right], \quad \rho_2 = \Gamma\left[\frac{1 - P_I}{\alpha\tau} - \frac{P_I}{\beta\tau}\right], \quad (21)$$

$$\sigma_i = \Gamma\left[\frac{1 - P_I}{\alpha\tau} + i\right], \quad \varepsilon_i = \Gamma\left[\frac{1 - P_I}{\alpha\tau} - \frac{P_I}{\beta\tau} + i\right], \qquad (22)$$

whereas $\Gamma[\cdot]$ is the Gamma function [*Abramowitz and Stegun*, 1965]. The expression of the standard deviation, σ_v, is given in Appendix B, while the third- and fourth-order moments are not reported due to space limitations.

[26] To obtain the analytical steady state solution of the stochastic model the time-dependent terms, $V_c = V_c(\delta(t))$ and $\alpha_1 = \alpha_1(h(t) - \eta)$, have been approximated with the respective average values defined by relationships (7). The influence of such approximations was tested by comparing the analytical results with the numerical simulation of the original model (2), and by investigating a wide range of hydrological and ecological conditions. Figures 3 and 4 show an example of these comparisons. This example refers to the case with $n = m = p = 1$, considering Salix Nigra as the riparian species, but the same behavior has been observed for all the other choices of the parameters. In particular, Figure 3 shows four comparisons of probability density functions of the vegetation biomass for different values of the inundation probability, P_I, while the scatterplot reported in Figure 4 compares the predicted and simulated expected values μ_v ($C_h = \mu_h/\sigma_h$ indicates the coefficient of variation of the water level). Figures 3 and 4 show an excellent agreement between model (2) and the simplified analytical model (9).

4. Riparian Vegetation Distribution Along a Transect

[27] The analytical framework developed in the previous section can be used to investigate the transversal distribution of the riparian vegetation. Two examples are shown in this section. We first discuss a simplified case where topography and river hydrology do not need to be specified; in this way, some general features of the vegetation distribution are discussed (section 4.1). We then consider a more specific case that refers to a class of rivers characterized by a quasi-trapezoidal transversal section (section 4.2). In both cases we assume $n = m = p = 1$.

[28] In the following, to avoid arbitrariness in setting a numeric value for K, we relate the ratio $k = K/\alpha_2$ to the ratio of vegetation timescales, T_g^* and T_d^*. Thus, under the above assumptions, considering $\langle h - \eta \rangle$ of order of magnitude of 1,

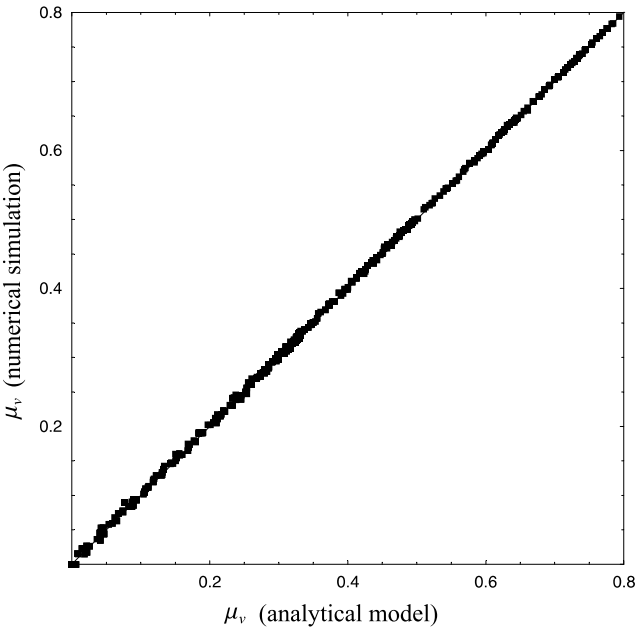

Figure 4. Comparison of the values of μ_v given by analytical expression (20) and obtained from numerical simulations. The points refer to the cases with hydrological and ecological parameters in the following ranges: $\tau = 10^{-3}$–1, $C_h = 0.4$–0.7, $k = 2.5$–10, and $P_I = 0.1$–0.9.

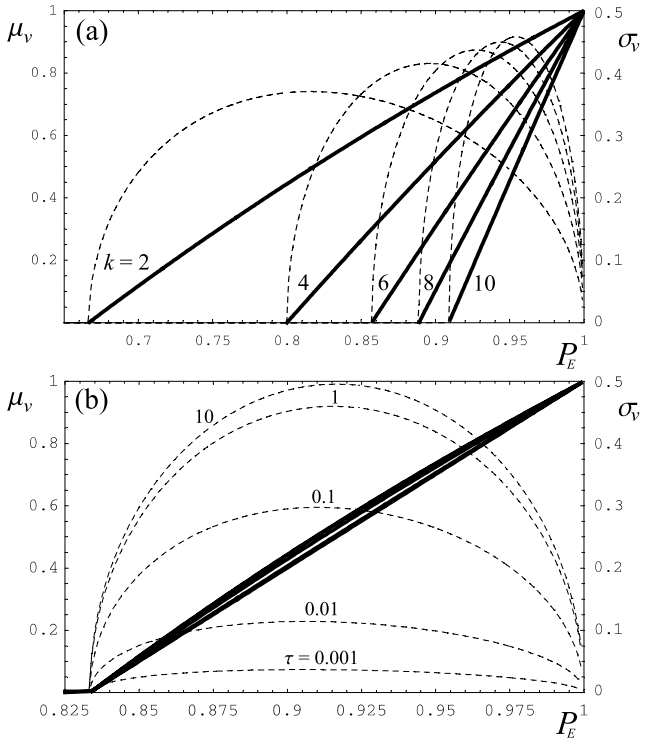

Figure 5. Case with $\alpha = k$ and $\beta = 1$. Behavior of the expected value, μ_v (thick line), and the standard deviation, σ_v (dashed line), as a function of exposure probability, P_E: (a) $\tau = 0.5$, $k = [2-10]$, and $\delta_{opt} = 0.25$ and (b) $\tau = [0.001-10]$, $k = 5$, and $\delta_{opt} = 0.25$.

and recalling the definition of T_d^* and T_g^* (see section 2), we obtain

$$T_d^* \simeq \int_{0.95}^{0.05} \frac{dv}{Kv} = \frac{2.94}{K}, \tag{23a}$$

$$T_g^* \simeq \int_{0.05}^{0.95} \frac{dv}{\alpha_2 v(1-v)} = \frac{5.88}{\alpha_2}, \tag{23b}$$

hence

$$k = \frac{K}{\alpha_2} \simeq \frac{T_g^*}{2T_d^*}, \tag{24}$$

namely the ratio between the decay and the growth coefficients is equal to half the ratio of the corresponding timescales. Generally, T_g^* is greater than T_d^*, thus $k > 2$.

4.1. Case With $\alpha = k$ and $\beta = 1$

[29] Let us assume that neither the decay rate (α_1) nor the carrying capacity (V_c) depend on the transversal position, x. From an ecological point of view, these conditions correspond to vegetation which (1) suffers from inundation, regardless of the magnitude of the floods and (2) tolerates large excursions of the phreatic surface. This implies that the carrying capacity is always close to the optimum value regardless of the groundwater level, as in the case of riparian species in humid areas which do not tap groundwater. It follows that $\alpha_1 = K = const$, $V_c = 1$, and therefore $\alpha = k$ and $\beta = 1$. Coherently, model (9a) and (9b) becomes

$$\frac{dv}{dt} = -kv^n \quad h \geq \eta \tag{25a}$$

$$\frac{dv}{dt} = v^m(1-v)^p \quad h < \eta, \tag{25b}$$

where the stochastic hydrological forcing only influences the switching between the evolution equations, through P_I, P_E, and τ, without affecting the value of the parameters of (25).

[30] The steady state pdf of model (25) and the corresponding moments are the same as those deduced in the previous section, with $\alpha = k$ and $\beta = 1$. In this case, because $p(v)$ retains its dependence on x only through P_E (or P_I), the statistics of v can be directly plotted as a function of the exposure probability, P_E, which is a hydrologically based proxy for the transversal coordinate, x. In this way, the effect of the flow variability on the vegetation distribution along the transect can be described in general form, without any knowledge of the details of $p(h)$.

[31] Figure 5 shows the dependence of the mean, μ_v, and standard deviation, σ_v, of vegetation biomass on the exposure probability, P_E. It is observed that the integral scale of the water levels, τ, does not significantly influence μ_v. The latter instead depends to a great extent on the ratio of decay and growth rate, k, and the exposure probability, P_E. Moreover, the soil remains unvegetated until P_E exceeds a threshold value that depends only on (i.e., increases with) k. Thus the exposure probability needs to exceed a threshold value for the growth phases to significantly affect vegetation dynamics. The high value of the threshold is due to the fact that the typical timescales of the vegetation decay are much shorter than the timescales of growth, as suggested by values of k greater than 2. For the same reason, even though in this case V_c is constant ($V_c = 1$) for any value of x, $\mu_v = 1$ only for $P_E = 1$, namely very far from the river. In fact, the random occurrence of even rare inundation events is always able to temporarily destroy part of the vegetation.

[32] The uniformity along the transect of the averaged value of the carrying capacity, β, implies a monotonic increase in the vegetation biomass, with the distance from the river. On the other hand, σ_v is never a monotonic function of the distance, regardless of the choice of the parameters. In fact, both for low (i.e., very close to the bank) and high values of P_E (i.e., far from the bank), $p(v)$ tends to a Dirac delta function, with $\sigma_v = 0$ and mean $\mu = 0$ and $\mu = 1$, respectively.

4.2. Quasi-trapezoidal Riparian Transects

[33] Let us consider the quasi-trapezoidal river section shown in Figure 6, which schematizes the transversal topography that can often be observed along alluvial rivers. To obtain an analytical expression of the probability distribution, $p(h)$, of the hydrologic forcing the following hypotheses are made (but a numerical form of $p(h)$ can be obtained for more complicated conditions). (1) Because the timescale of the flow variability is much longer than the hydrodynamic timescale, the flow can be considered quasi-steady. It follows that the local depth-averaged velocity satisfies Chezy's law throughout the cross section [*Henderson*,

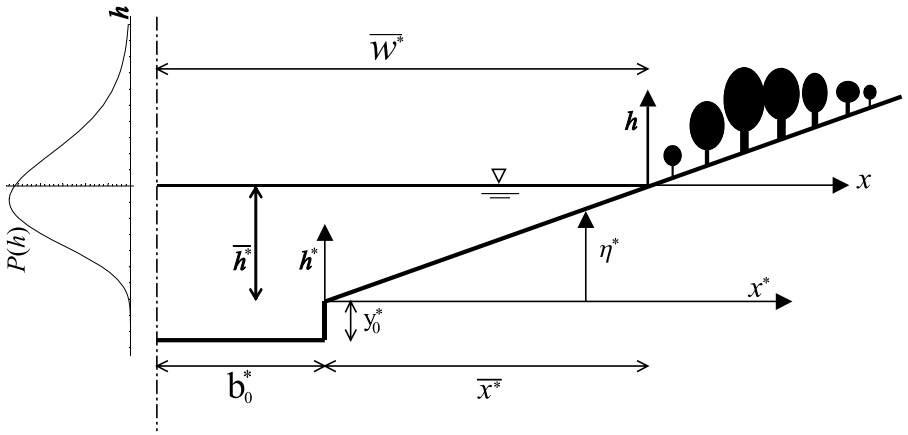

Figure 6. Sketch of the cross section of a quasi-trapezoidal transect.

1966]; (2) two constant values of Manning friction coefficient (n_r and n_f) are assumed for the central zone of the river bed and the riparian zone, respectively [*Pettit et al.*, 2001]; (3) the phreatic surface is assumed to be horizontal, so that $\zeta = h$. Although not required by our analytical approach, this third assumption is justified by the relatively small slopes of the water table in the transverse direction.

[34] We assume that flow discharge, Q, follows a lognormal distribution, $p(Q)$ [*Bras*, 1990; *Maidment*, 1993]. Without any loss of generality, we define

$$\bar{Q} = cQ_0, \quad \sigma_Q = C_Q\bar{Q} = cC_QQ_0, \tag{26}$$

where the subscript "0" refers to the minimum water levels (i.e., $h^* = 0$), c is a coefficient greater than unity, and $\bar{Q}$, σ_Q, and C_Q are the mean, standard deviation, and coefficient of variation of the river discharges, respectively. As $p(Q)$ is lognormal, the pdf of the (dimensioned) water level in the river is

$$p(h^*) = p(Q)\frac{dQ}{dh^*} = \frac{1}{\sqrt{2\pi}\sigma(Q-Q_0)}e^{-\frac{1}{2}\left(\frac{\ln(Q-Q_0)-\varsigma}{\nu}\right)^2}\cdot\frac{dQ}{dh^*} \tag{27}$$

where

$$\varsigma = \ln\frac{(\bar{Q}-Q_0)^2}{\sqrt{(\bar{Q}-Q_0)^2+\sigma_Q^2}}, \tag{28a}$$

$$\nu = \sqrt{\ln\left(1+\frac{\sigma_Q^2}{(\bar{Q}-Q_0)^2}\right)}. \tag{28b}$$

[35] Under the previously mentioned hydraulic hypotheses, the following relationship between the discharge and the water table level can be obtained

$$Q = 2\sqrt{I_r}\left[\frac{b_0^*}{n_r}\left(h^*+y_0^*\right)^{\frac{5}{3}}+\frac{1}{n_f}\int_0^{h^*/I_t}(h^*-I_tx^*)^{\frac{5}{3}}dx\right], \tag{29}$$

where I_t is the slope of the riparian transect, I_r is the longitudinal river slope, y_0^* is the stream depth at the minimum water conditions, and b_0^* is the half width of the central zone of the river bed where the minimum discharge flows (see Figure 6). Moreover, from the dimensionless notation (1) in the present case, we obtain $\eta^*/x^* = \bar{h}/\bar{x} = I_t$ and hence $\eta \equiv x$.

[36] By substituting equation (29) in (27) we obtain

$$p(h^*) = \frac{4\sqrt{2}\left[5\left(h^*+y_0^*\right)^{\frac{2}{3}}b_0^*n_f+\frac{3h^{*\frac{5}{3}}n_r}{I_t}\right]e^{\frac{\Lambda^2}{2\varsigma^2}}}{3\sqrt{\pi}\varsigma\left[8\left(h^*+y_0^*\right)^{\frac{5}{3}}b_0^*n_f+\left(3(h^*)^{\frac{8}{3}}-\frac{4Q_0n_f}{\sqrt{I_r}}\right)n_r\right]}, \tag{30}$$

with

$$\Lambda = \nu - \ln\left[2\sqrt{I_r}\left(\frac{3h^{*\frac{8}{3}}}{8I_tn_f}+\frac{\left(h^*+y_0^*\right)^{\frac{5}{3}}b_0^*}{n_r}\right)-Q_0\right]. \tag{31}$$

[37] A sensitivity analysis was performed to test the dependence of equation (30) on all the hydraulic and geometric parameters. The parameters were in particular monitored in the following intervals: $C_Q \in [0.2-1.4]$, $(I_r, I_t) \in [10^{-3}-10^{-2}]$, $c \in [2-10]$, $n_r \in [20-35]\ m^{-1/3}s$, $n_f \in [15-25]\ m^{-1/3}s$, $y_0^* \in [0.3-1.5]\ m$, and $b_0^* \in [5-20]\ m$. It was found that (1) the coefficient of variation of the water levels, C_h, is limited to the range [0.25–0.75] and (2) the pdf of dimensionless water levels, $p(h)$, is very well represented by a standard Gamma distribution which, using dimensionless variables, reads

$$\wp(h) = \frac{1}{\Gamma(\lambda)}\lambda^\lambda(1+h)^{\lambda-1}e^{-\lambda(1+h)}, \tag{32}$$

where $\lambda = 1/C_h^2$. The latter point was proven by means the computation of the norm

$$|p(h), \wp(h)| = \sqrt{\int_{-1}^{\infty}(p(h)-\wp(h))^2dh}, \tag{33}$$

which gives an indication of the distance between functions $p(h)$ and $\wp(h)$. We always obtained $|p, \wp| < 0.01$ for each parameter combination, and therefore, for the sake of simplicity, we used the Gamma distribution in place of the actual pdf (30). As a consequence, $p(h) \simeq \wp(h)$ results to be

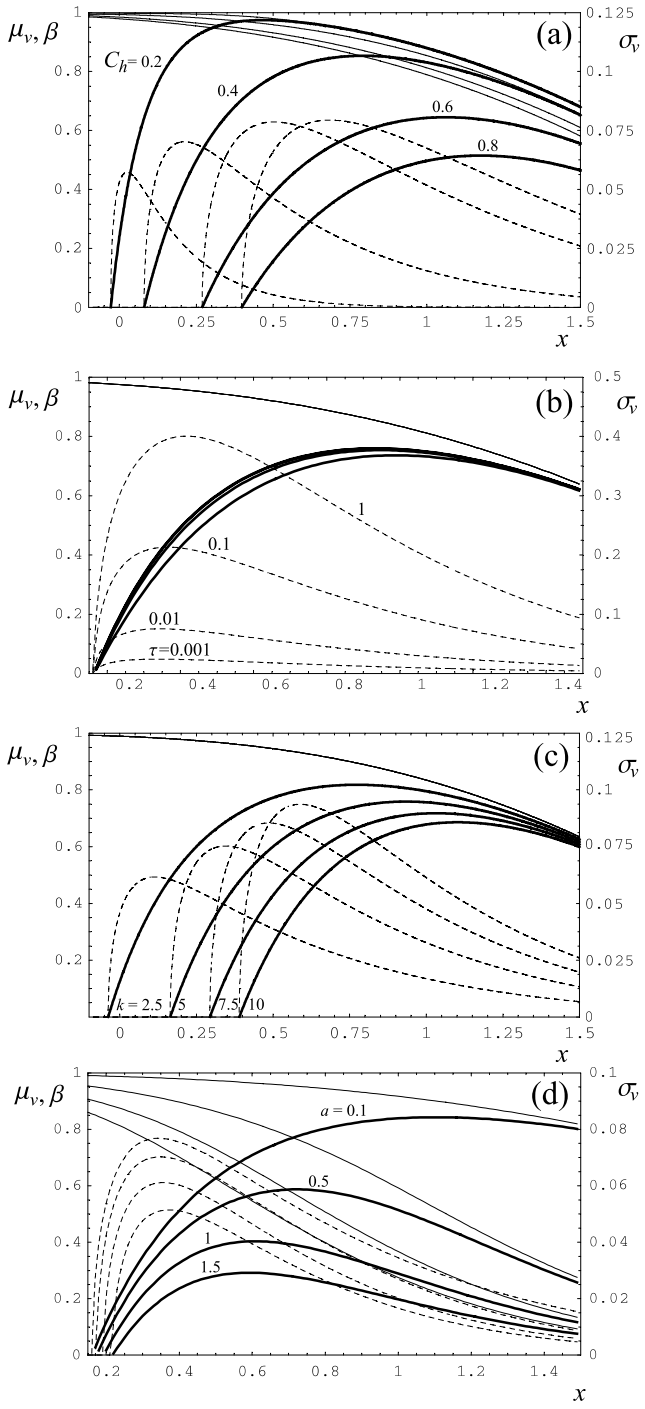

Figure 7. Distribution along the transect of the mean value (μ_v, thick lines), the averaged carrying capacity (β, thin lines), and the standard deviation (σ_v, dashed lines) of the vegetation biomass. (a) C_h = [0.2–0.8], (b) τ = [0.001–1], (c) k = 2.5–10, and (d) a = [0.1–1.5].

only described by C_h, which, along with the integral scale, τ, completes the set of parameters and functions needed to describe the hydrologic forcing.

[38] The transversal distributions of μ_v and σ_v are shown in Figures 7a–7d along with the dependence on hydrologic (C_h, τ) and biological (k, a) parameters that affect the dynamics.

[39] The average value of vegetation biomass varies along the x direction from zero close to the river, up to a maximum value and, then, it slowly decreases asymptotically approaching the average value of carrying capacity, $\beta(x)$, at high x. This behavior differs from the simplified case shown in Figure 5 due to two different factors. On the one hand, the monotonic decrease in the carrying capacity along x direction forces vegetation biomass, v, to decrease with increasing distances from the river bank. On the other hand, inundations frequently destroy vegetation close to the river. It follows that a maximum of the average value of the vegetation biomass will occur at a particular location, $x = x_M$. Conversely, the dependence of σ_v on x (see Figure 7) maintains the same features discussed in section 4.1, apart from the fact that some curves lose the symmetry shown in Figure 5 because of the nonlinear transformation between P_E and x.

[40] As far as the role of the hydrologic parameters is concerned, Figures 7a and 7b show the effect of the coefficient of variation, C_h, and the autocorrelation time, τ, of the water levels, respectively. C_h affects both the location of the vegetated zone and the peak value; in particular, the riparian vegetation shifts outward and the overall mean amount of riparian biomass (i.e., $\int_{-1}^{\infty} \mu_v \, dx$) decreases when the discharge variability increases, because of the increasing occurrence of inundation events. Instead, the maximum value of σ_v remains almost constant. Conversely, different correlations do not lead to significant changes in the mean value of $p(v)$, but significantly affect its shape, as shown by the standard deviation. In particular, σ_v increases with the autocorrelation of the hydrologic forcing. In fact, an increase in τ corresponds to an increase in the mean duration of exposure and inundation phases, so the system is more likely close to the extreme stationary states, i.e., at $v = 0$ and $v = \beta$.

[41] The role played by the biological parameters is shown in Figures 7c and 7d through the dependence on k and a. The former parameter influences μ_v in a similar way as C_h: when k is high, the tolerance to the water stress by inundation decreases so the riparian zone shifts outward with a consequent increase in the unvegetated zone close to the river. However, in this case, the standard deviation increases with k. Conversely, an increment in coefficient a, which determines the range of water table depths tolerated by phreatophyte (see equations (6), (5)), induces a decrease both in μ_v and σ_v, and just a weak shift in the vegetated zone. An increase in a implies in fact a reduction of the growth phases, although the total time of exposure is unchanged.

[42] It is also useful to make some comparisons of the different vegetation species. For example, we considered the six bottomland hardwood species listed in Table 1, with values of D_m, H_m and T_m^* taken from *Pearlstine et al.* [1985]. The coefficients α_2 have been calculated for each species using the JABOWA model, as described in section 2, whereas the decay coefficient K was conventionally assumed equal to 0.0028 days^{-1} irrespective of the species, for the sake of simplicity. In short, three dimensionless parameters change with the vegetation: $k = K/\alpha_2$, $\delta_{opt} = \delta^*_{opt}/\bar{h}$, and $\tau = \alpha_2 \tau^*$.

[43] The behavior of the mean vegetation biomass along the transect is reported in Figure 8, where the picture does

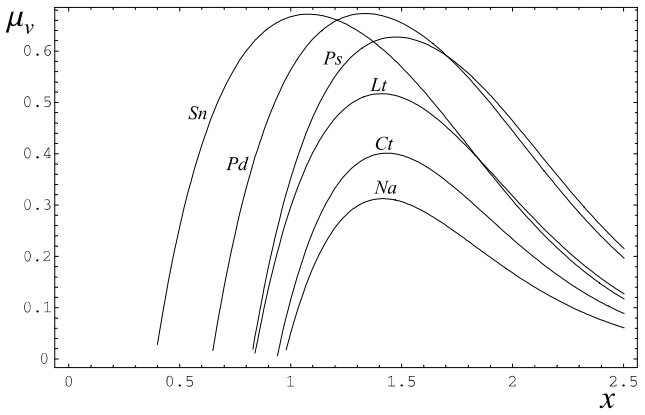

Figure 8. Behavior of the expected value of the biomass along the riparian transect for different species: *Carya tomentosa* (*Ct*), *Liriodendron tulipifera* (*Lt*), *Nyssa aquatica* (*Na*), *Populus deltoides* (*Pd*), *Prunus serotina* (*Ps*), and *Salix nigra* (*Sn*). (C_h = 0.5, τ^* = 30 days, $\overline{h^*}$ = 2 m, and α_1 = 0.0028.)

not describe a community of coexistent individuals (the interspecies interactions are not accounted for in our model) but rather different scenarios that correspond to single species. Figure 8 clearly shows that both the extent of the unvegetated zone and the fraction of biomass, with respect to optimal steady conditions (v is dimensionless) change significantly with the species. In particular, the model reproduces the tendency of *Salix* and *Populus* to grow close to the river [*Naiman and Decamps*, 1997]: due to their endurance and resistance to flooding, these species can stand a broad range of hydrological regimes. This explains the recognized competitive advantage of these species in the colonization of bare soil subsequent to sedimentation processes [e.g., *Hughes*, 1997].

[44] Further, the width of the unvegetated zone can be investigated, using the limit condition imposed by equation (19), which can be solved with respect to x under the hydraulic and geometric conditions considered in this case. The boundary of the riparian zone, $x = x_{inf}$, is found to increase monotonically with C_h, as shown in Figure 9, irrespective of the value of τ.

5. Discussion and Conclusions

[45] Riparian corridors are complex ecotones regulated by processes acting longitudinally (along the stream), laterally (along the transect), vertically (toward the groundwater), and in time [*Tockner et al.*, 2000]. In our model we have focused on lateral and vertical directions and time, by stochastically modeling the main ecohydrologic processes affecting the control exerted by flow variability on riparian ecosystems. In a similar way to other ecohydrological studies in vegetation ecosystems (e.g., [*Rodriguez-Iturbe*, 2000; *Porporato and Rodriguez-Iturbe*, 2002; *D'Odorico et al.*, 2004, 2005; *Rodriguez-Iturbe and Porporato*, 2005]), our aim was to quantitatively investigate how stream and near-stream hydrology is able to impact ecological processes. In this section, we discuss the limits and reliability of our modeling approach, in the light of some field studies.

[46] The level of completeness of the analytical model developed in the previous sections is summarized in Table 2, where both the considered and neglected processes are listed. Table 2 refers to the fundamental hydrogeomorphological factors that affect the riparian habitat, according to a recent review by *Steiger et al.* [2005]. The quantities used in our modeling framework are also reported in the same table. It confirms that several important aspects have been focused on and modeled. In particular, we considered all the main processes involving the hydrological and hydraulic characteristics of the river and the properties of riparian vegetation. Some aspects linked to woody debris, the effects of external forcings, and fluvial geomorphology instead were not considered. The latter is probably the most important one. Although some field studies have shown that sediment size characteristics can be of secondary importance [*Osterkamp and Hupp*, 1984], other geomorphological processes such as erosion and sedimentation play an important role in the interaction with riparian vegetation and the consequent change in the riparian topography. Thus the main limitation of the present modeling approach is that it assumes the transect topography to be time-independent. This assumption precludes the application of our results to environments that develop high lateral migration rates, as is the case of very tortuous meandering rivers. Conversely, slightly sinuous planimetry permit the above results to be adopted, provided the timescale of river migration is longer than the time scale of the vegetation dynamics.

[47] One of the main results of our analytic formulation is the description of the river-induced lateral distribution of riparian vegetation. A rigorous quantitative comparison with real riparian communities is very difficult since the literature on riparian systems, though wide and varied, rarely provides all the hydrological and biologic data necessary for a rigorous comparison with our model-based results. Furthermore, field studies usually investigate the transient response of vegetation to a man-induced change in the flow regime (e.g., dam regulation), rather than the long-term steady state. Nevertheless, a qualitative comparison is still possible on the basis of the results of several studies on the dependence of riparian vegetation biomass on the distance from the channel

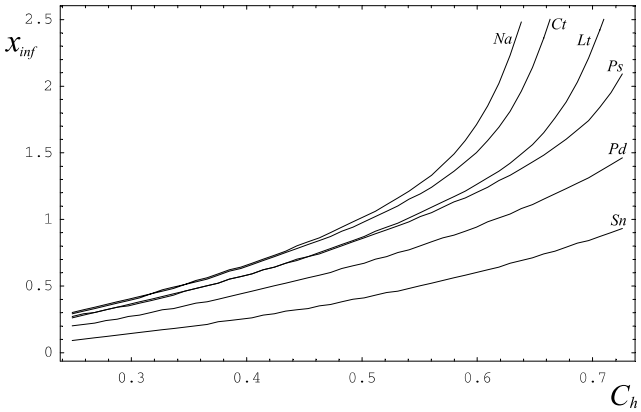

Figure 9. Position of the lowest vegetated site versus C_h according to the condition (19).

Table 2. Primary Factors Interacting at the Local Scale[a]

Considered	Neglected
Flood event characteristics: frequency (P_I, C_Q), intensity ($h - \eta$), duration (τ), alternation of inundation exposure ($\xi(t)$)	Geomorphic properties: erosion and sedimentation, mosaic of fluvial landforms, grain size of sediment deposits
Flow hydraulics: water depth ($h - \eta$), shear stress ($K(h - \eta)$), water table ($\zeta(x, t)$), different roughness of the river bed and floodplain (n_r, n_f)	Flow hydraulics: local flow directions, heterogeneity in the roughness, time delay between the river and groundwater table
Geomorphic properties: topography ($\eta(x)$)	Properties of dead wood: size of dead wood accumulations, density of dead wood accumulations
Properties of living vegetation: species present (m, n, p, K, α_2), vegetation cover ($v(x, t)$), aboveground biomass, density ($v(x, t)$)	External forcings: water quality, climate change and herbivory

[a]Modified from data of *Steiger et al.* [2005]. The corresponding components of the model are reported in the parentheses.

[e.g., *Nanson and Beach*, 1977; *Hupp and Osterkamp*, 1985; *Bradley and Smith*, 1986; *Richter and Richter*, 2000]. In agreement with our results, peaked lateral distributions have been very frequently observed along riparian transects. For example, *Johnson et al.* [1995] investigated the occurrence of different types of vegetation along the Snake River (Idaho) as a function of plot elevation. A modified diagram of their results is given in Figure 10a. The transversal distribution of trees, forb shrubs, and transitional species shows typical peaked behavior, where both the position of the peak and the lateral extension of the habitat depend on the type of vegetation. *van Coller* [1993] described a similar distribution and abundance of mature individuals as a function of the elevational gradient of the Sabie River riparian forest (see Figure 10b). *Lytle and Merritt* [2004], through a numerical probabilistic model, also found that the cottonwood density peaks at intermediate levels of flood frequency (corresponding here to P_I). All these features qualitatively validate the results of our model (see Figure 8).

[48] The existence of a strip where riparian (phreatophyte) species develop, and where the interior and exterior margins are marked by hydrological processes, is easily recognizable along riparian corridors. Figures 11a and 11b show two examples, where the presence of a peak in vegetation density is also visible. The not monotonic behavior of the riparian vegetation distribution is due to the negative action (1) of floods, at plots close to the river, and (2) to a too deep phreatic surface, far from the river. In contrast, upland vegetation, which is not phreatophyte, is only affected by flood disturbance, which decreases in magnitude with an increasing distances from the river bank, while its carrying capacity does not depend on the depth of the water table (i.e., β = const). It follows that a monotonic increasing lateral distribution occurs, in agreement with the case discussed in section 4.1 (Figure 5). The outcome of this model is also confirmed by examining field data by *Johnson et al.* [1995] (see Figure 10a). Very similar findings were also presented by *Auble et al.* [1994]; they investigated the dependence of the distribution of some herbaceous species on the probability P_I, and detected a monotonic behavior that closely resembles the pattern described by our model in Figure 5.

[49] Several studies have pointed out the necessity of matching quantitative information of a functional response of riparian vegetation with quantitative information on the

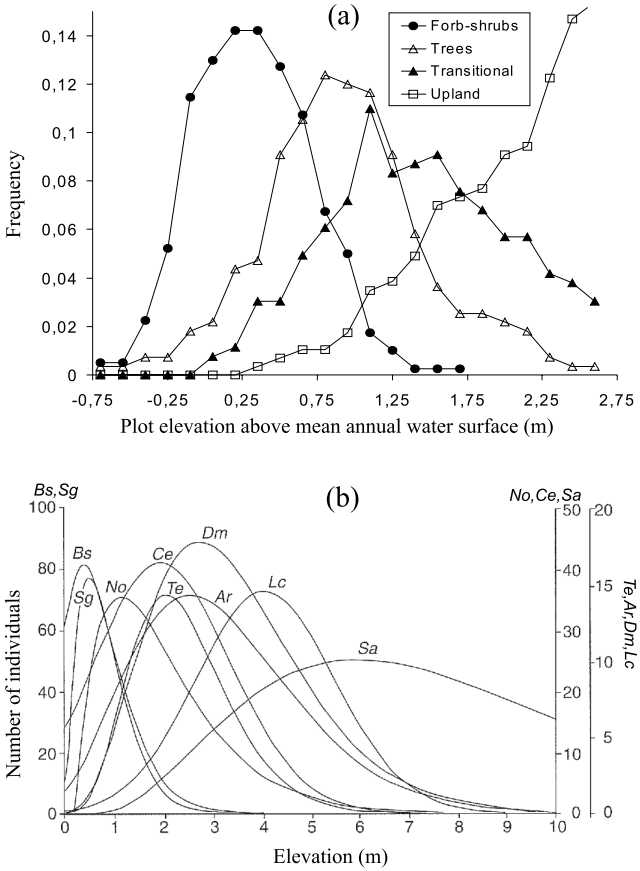

Figure 10. Examples of lateral distributions of riparian vegetation. (a) Frequency of occurrence versus elevation above mean water level of the Snake River (Idaho). Modified from *Johnson et al.* [1995]. (b) Abundance of mature individuals of selected tree species ($D^* > 3$ cm) versus elevation of Sabie River riparian corridor (South Africa): *Breonadia salicina* (Bs), *Syzygium guineense* (Ar), *Nuxia appositifolia* (No), *Combretum erythrophyllum* (Ce), *Trichilia emetica* (Te), *Acacia Robusta* (Ar), *Diospyros mespiliformis* (Dm), *Lonchocarpus capassa* (Lc), and *Spirostachys africana* (Sa). Reprinted from *Naiman et al.* [2005]. Copyright (2005), with permission from Elsevier.

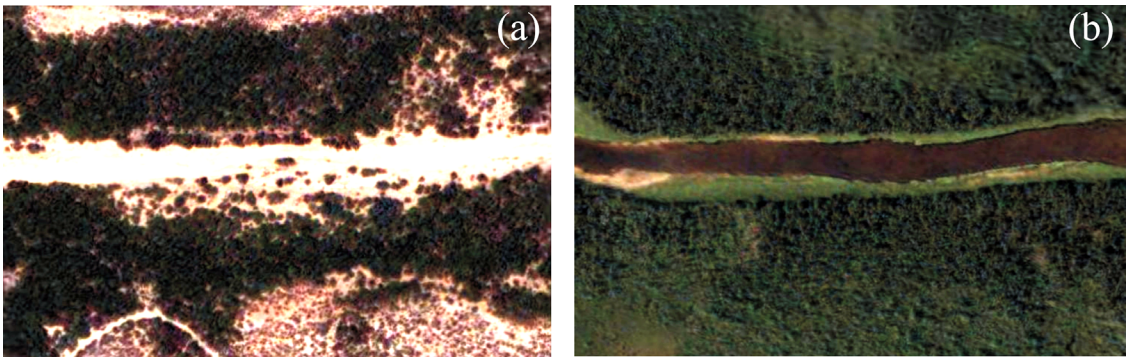

Figure 11. Two examples of riparian corridors. (a) San Pedro River (Arizona) 32°07′53″N, 110°17′17″W. (b) Kinoje River (Ontario) 51°58′19″N, 81°39′34″W. Reprinted with permission from DigitalGlobe and Google Earth.

river hydrology [e.g., *Scott et al.*, 1999; *Lytle and Merritt*, 2004]. The present work is an attempt in this direction, and it provides some process-based analytical tools to investigate the coupled ecosystem-hydrologic dynamics in riparian ecosystems. We are aware that some simplifying hypotheses have been made, but this was necessary to maintain the model both mathematically tractable and parsimonious. However, we believe that several fundamental processes have been properly taken into account and the resulted obtained with our closed form solutions are qualitatively consistent with field observations. The proposed model shows that rather simple interactions can produce complex patterns and, although this novel approach is not yet suitable for use in management and restoration of fluvial landscapes, it can be considered a starting point for subsequent works that address the stochastic features of the riparian vegetation dynamics.

Appendix A: Some Analytical Expressions of the pdf, $p(v)$

[50] Analytical solutions for steady vegetation biomass pdf are available for several different combinations of the exponents m, n, and p. In particular, here we report the cases with $p = m$, for which

$$p(v) = \frac{N}{\alpha}\frac{\alpha v^n + v^m(\beta - v)^m}{(\beta - v)^m v^{m+n}} e^{\frac{v^{1-n}(P_I-1)}{(n-1)\alpha\tau} + \frac{{}_2F_1\left[1-m,m;2-m;\frac{v}{\beta}\right]P_I}{(m-1)\tau\beta^m v^{m-1}}} \tag{A1}$$

if m is not an integer and $n \neq 1$,

$$p(v) = \frac{N}{\alpha}\frac{\alpha v^n + v^m(\beta - v)^m}{(\beta - v)^m v^{\frac{P_I+1}{\alpha\tau}}} v^{m+1} e^{\frac{{}_2F_1\left[1-m,m;2-m;\frac{v}{\beta}\right]P_I}{(m-1)\tau\beta^m v^{m-1}}} \tag{A2}$$

if m is not an integer and $n = 1$, and

$$p(v) = \frac{N}{\alpha}\frac{(v-\beta)^{\frac{P_I}{\beta\tau}-1}}{v^{\frac{P_I}{\beta\tau}+n+1}}\left(v^n\alpha - v^2 + \beta v\right)e^{\frac{v^{1-n}(P_I-1)}{(n-1)\alpha\tau}} \tag{A3}$$

if $m = 1$ and $n \neq 1$.

[51] In the previous expressions, ${}_2F_1[a, b; c, d]$ is the Hypergeometric function (*Abramowitz and Stegun* [1965]).

Appendix B: Analytical Expression of the Standard Deviation When $m = n = p = 1$

[52] Starting from expressions (18), the second-order central moment, μ_2, is given by

$$\mu_2 = \frac{\beta^2\rho_1}{(\beta\varepsilon_1\rho_1 - \rho_0\rho_2\sigma_1)^2\sigma_2^2\sigma_3}\left[\beta\varepsilon_1\rho_1\sigma_1\sigma_2(\beta\varepsilon_3\sigma_2 + \varepsilon_2\rho_0\sigma_3) - \left(\varepsilon_1{}^2\rho_0{}^2\rho_1\sigma_2{}^2\sigma_3\right) - \sigma_1{}^2\left(\beta\varepsilon_3\rho_0\rho_2\sigma_2{}^2 + \varepsilon_2\left(\beta^2\varepsilon_2\rho_1 - \rho_0{}^2\rho_2\sigma_2\right)\sigma_3\right)\right] \tag{B1}$$

from which $\sigma_v = \sqrt{\mu_2}$.

[53] **Acknowledgment.** The authors wish to thank Cliff Hupp and the two anonymous reviewers for their suggestions and are grateful to the Regione Piemonte, the Cassa di Risparmio di Cuneo (CRC), and the Cassa di Risparmio di Torino (CRT) Foundations for their financial support.

References

Abramowitz, M., and I. A. Stegun (1965), *Handbook of Mathematical Functions: With Formulas, Graphs and Mathematical Tables*, Dover, Mineola, N. Y.

Auble, G. T., J. M. Friedman, and M. L. Scott (1994), Relating riparian vegetation to present and future streamflows, *Ecol. Appl.*, *4*(3), 544–554.

Baskerville, G. L. (1965), Dry matter production in immature balsam fir stands, *For. Sci. Monogr.*, *9*, 1–42.

Bendix, J., and C. R. Hupp (2000), Hydrological and geomorphological impacts on riparian plant communities, *Hydrol. Processes*, *14*, 2977–2990.

Botkin, D. B., J. F. Janak, and J. R. Wallis (1972), Some ecological consequences of a computer model of forest growth, *J. Ecol.*, *60*, 849–872.

Bradley, C. E., and D. G. Smith (1986), Plains cottonwood recruitment and survival on a prairie meandering river floodplain, Milk River, southern Alberta and northern Montana, *Can. J. Bot.*, *64*, 1433–1442.

Bras, R. L. (1990), *Hydrology: An Introduction to Hydrologic Science, Addison-Wesley*, Reading, Mass.

Brookes, C. J., J. M. Hooke, and J. Mant (2000), Modelling vegetation interactions with channel flow in river valley of the Mediterranean region, *Catena*, *40*, 93–118.

Camporeale, C., P. Perona, A. Porporato, and L. Ridolfi (2005), On the long-term behavior of meandering rivers, *Water Resour. Res.*, *41*, W12403, doi:10.1029/2005WR004109.

D'Odorico, P., A. Porporato, F. Laio, L. Ridolfi, and I. Rodriguez-Iturbe (2004), Probabilistic modeling of nitrogen and carbon dynamics in water-limited ecosystems, *Ecol. Modell.*, *179*(2), 205–219.

D'Odorico, P., F. Laio, and L. Ridolfi (2005), Noise-induced stability in dryland plant ecosystems, *Proc. Natl. Acad. Sci. U. S. A.*, *102*(31), 10,819–10,822.

Franz, E. H., and F. A. Bazzaz (1977), Simulation of vegetation response to modified hydrologic regimes: A probabilistic model based on niche differentiation in a floodplain forest, *Ecology*, *58*, 176–183.

Friedman, J. M., and G. T. Auble (1999), Mortality of riparian box elder from sediment mobilization and extended inundation, *Reg. Rivers Res. Manage.*, *15*, 463–476.

Gurnell, A., G. E. Petts, D. M. Hannah, B. P. G. Smith, P. J. Edwards, J. Kollmann, J. V. Ward, and K. Tockner (2001), Riparian vegetation and island formation along the gravel-bed fiume Tagliamento, Italy, *Earth Surf. Processes Landforms*, *26*, 31–62.

Henderson, F. M. (1966), *Open Channel Flow*, MacMillan, New York.

Hughes, F. M. R. (1997), Floodplain biogeomorphology, *Progr. Phys. Geogr.*, *21*, 501–529.

Hunt, R. (1982), *Plant Growth Curves*, Univ. Park Press, Baltimore, Md.

Hupp, C. R. (1988), Plant ecological aspects of flood geomorphology and paleoflood history, in *Flood Geomorphology*, edited by V. R. Baker, R. C. Kochel, and P. C. Patton, pp. 335–356, John Wiley, Hoboken, N. J.

Hupp, C. R., and W. R. Osterkamp (1985), Bottomland vegetation distribution along Passage Creek, Virginia, in relation to fluvial landforms, *Ecology*, *66*(3), 670–681.

Ikeda, S., and G. Parker (Eds.) (1989), *River Meandering*, *Water Res. Monogr. Ser.*, vol. 12, AGU, Washington, D. C.

Johnson, W. C. (2000), Tree recruitment and survival in rivers: Influences of hydrological processes, *Hydrol. Processes*, *14*, 3051–3074.

Johnson, W. C., M. D. Dixon, R. Simons, S. Jenson, and K. Larson (1995), Mapping the response of riparian vegetation to possible flow reductions in the Snake River, Idaho, *Geomorphology*, *13*, 159–173.

Jones, J. B., and P. J. Mulholland (2000), *Streams and Ground Waters*, Elsevier, New York.

Kitahara, K. T., W. Horsthemke, R. Lefever, and Y. Inaba (1980), Phase diagrams of noise induced transitions, *Prog. Theor. Phys.*, *64*(4), 1233–1247.

Kot, M. (2001), *Elements of Mathematical Ecology*, Cambridge Univ. Press, New York.

Kozlowski, T. T. (1984), Responses of woody plants to flooding, in *Flooding and Plant Growth*, edited by T. T. Kozlowski, pp. 129–163, Elsevier, New York.

Lite, S. J., K. J. Bagstad, and J. C. Stromberg (2005), Riparian plant species richness along lateral and longitudinal gradients of water stress and flood disturbance, San Pedro River, Arizona, USA, *J. Arid. Environ.*, *63*, 785–813.

Liu, J., and P. S. Ashton (1995), Individual based simulation models for forest succession and management, *For. Ecol. Manage.*, *73*, 157–175.

Lytle, D. A., and D. M. Merritt (2004), Hydrologic regimes and riparian forests: A structured population model for cottonwood, *Ecology*, *85*(9), 2493–2503.

Mahoney, J. M., and S. B. Rood (1998), Streamflow requirements for cottonwood seedling recruitment: An integrative model, *Wetlands*, *18*, 634–645.

Maidment, D. R. (1993), *Handbook of Hydrology*, McGraw-Hill, New York.

McKenney, R., R. B. Jacobson, and R. C. Wertheimer (1995), Woody vegetation and channel morphogenesis in low-gradient, gravel-bed streams in the Ozark Plateaus, Missouri and Arkansas, *Geomorphology*, *13*, 175–198.

Mitsch, W. J., and J. Gosselink (2000), *Wetlands*, 3rd ed., John Wiley, New York.

Naiman, R. J., and H. Decamps (1997), The ecology of interfaces: Riparian zones, *Annu. Rev. Ecol. Syst.*, *28*, 621–658.

Naiman, R. J., H. Decamps, and M. E. McClain (2005), *Riparia*, Elsevier, New York.

Nanson, G. C., and H. F. Beach (1977), Forest succession and sedimentation on a meandering-river floodplain, north east British Columbia, Canada, *J. Biogeogr.*, *4*, 229–251.

Nanson, G. C., S. Tooth, and D. Knighton (2002), A global perspective on dryland rivers: Perceptions, misconceptions and distinctions, in *Dryland River: Hydrology and Geomorphology of Semi-arid Channels*, edited by L. J. Bull and M. J. Kirby, pp. 17–54, John Wiley, Hoboken, N. J.

Naumburg, E., R. Mata-Gonzales, R. G. Hunter, T. McLendon, and D. W. Martin (2005), Phreatophytic vegetation and groundwater fluctuations: A review of current research and application of ecosystem response modeling with an emphasis on great basin vegetation, *Environ. Manage.*, *35*(6), 726–740.

Osterkamp, W. R., and J. E. Costa (1987), Change accompanying an extraordinary flood on sandbed stream, in *Catastrophic Flooding*, edited by L. Mayer and D. Nash, pp. 201–224, Allen and Unwin, St. Leonards, N. S. W., Australia.

Osterkamp, W. R., and C. R. Hupp (1984), Geomorphic and vegetative characteristics along three northern Virginia streams, *Geol. Soc. Am. Bull.*, *95*, 1093–1101.

Pearlstine, L., H. McKellar, and W. Kitchens (1985), Modelling the impacts of a river diversion on bottomland forest communities in the Santee River Floodplain, South Carolina, *Ecol. Modell.*, *29*, 283–302.

Perry, T. O., H. E. Sellers, and C. O. Blanchard (1969), Species-diversity and pattern-diversity in the study of ecological succession, *J. Theor. Biol.*, *10*, 370–383.

Perucca, E., C. Camporeale, and L. Ridolfi (2006), Influence of river meandering dynamics on riparian vegetation pattern formation, *J. Geophys. Res.*, *111*, G01001, doi:10.1029/2005JG000073.

Pettit, N. E., R. H. Froend, and P. M. Davies (2001), Identifying the natural flow regime and the relationship with riparian vegetation for two contrasting Australian rivers, *Regul. Rivers Res. Manage.*, *17*, 201–215.

Phipps, R. L. (1979), Simulation of wetland forest dynamics, *Ecol. Modell.*, *7*, 257–288.

Porporato, A., and I. Rodriguez-Iturbe (2002), A challenging multidisciplinary research perspective, *Hydrol. Sci. J.*, *47*(5), 811–821.

Richards, K., J. Brasington, and F. Hughes (2002), Geomorphic dynamics of floodplains, *Freshwater Biol.*, *47*, 559–579.

Richter, B. D., and H. E. Richter (2000), Prescribing flood regimes to sustain riparian ecosystem along meandering rivers, *Conserv. Biol.*, *14*, 1467–1478.

Ridolfi, L., P. D'Odorico, and F. Laio (2006), Effect of vegetation–water table feedbacks on the stability and resilience of plant ecosystems, *Water Resour. Res.*, *42*, W01201, doi:10.1029/2005WR004444.

Rodriguez-Iturbe, I. (2000), Ecohydrology: A hydrologic perspective of climate-soil-vegetation dynamics, *Water Resour. Res.*, *36*(1), 3–9.

Rodriguez-Iturbe, I., and A. Porporato (2005), *Ecohydrology of Water Controlled Ecosystems*, Cambridge Univ. Press, New York.

Scott, M. L., P. B. Shafroth, and G. T. Auble (1999), Responses of riparian cottonwoods to alluvial water table declines, *Environ. Manage.*, *23*, 347–358.

Shugart, H., and D. C. West (1977), Development of an Appalachian deciduous forest succession model and its application to assessment of the impact of the chestnut blight, *J. Environ. Manage.*, *5*, 161–179.

Steiger, J., E. Tabacchi, S. Dufour, D. Corenblit, and J. L. Peiry (2005), Hydrogeomorphic processes affecting riparian habitat within alluvial channel-floodplain river systems: A review for the temperate zone, *River Res. Appl.*, *21*, 719–737.

Stevens, J. A., and G. L. Waring (1985), The effects of prolonged flooding on the riparian plant community in Grand Canyon, in *Riparian Ecosystems and Their Management: Reconciling Conflicting Uses. First North American Riparian Conference*, edited by R. R. Johnson et al., pp. 81–86, U.S. Dep. of Agric., Fort Collins, Colo.

Stromberg, J. C. (2001), Restoration of riparian vegetation in the southwestern United States: Importance of flow regimes and fluvial dynamism, *J. Arid Environ.*, *49*, 17–34.

Stromberg, J. C., and D. T. Patten (1991), Instream flow requirements for cottonwoods at Bishop Creek, Inyo County, California, *Rivers*, *2*, 1–11.

Tockner, K., F. Malard, and J. V. Ward (2000), An extension of the flood pulse concept, *Hydrol. Processes*, *14*, 2861–2883.

van Coller, A. L. (1993), Riparian vegetation of the Sabie River: Relating spatial distribution patterns to characteristics of the physical environment, M.S. thesis, Univ. of Witwatersrand, Johannesburg.

Van Den Broeck, C. (1983), On the relation between white shot noise, Gaussian white noise, and dichotomic Markov process, *J. Stat. Phys.*, *31*(3), 467–483.

Van Kampen, N. (1992), *Stochastic Processes in Physics and Chemistry*, Elsevier, New York.

Yanosky, T. M. (1982), Effects of flooding upon woody vegetation along parts of the Potamac River flood plain, *U.S. Geol. Surv. Prof. Pap.*, *1206*.

Young, H. E., J. H. Ribe, and K. Wainwright (1980), Weight tables for tree and shrub species in Maine, *Misc. Rep. 230*, Univ. of Maine, Orono.

C. Camporeale and L. Ridolfi, DITIC, Politecnico di Torino, Corso Duca degli Abruzzi 24, I-10129 Torino, Italy. (carlo.camporeale@polito.it)